Optimal strategy in integrated energy system combining liquid air storage and waste heat utilization in power system

K. Wang[1], B. Cai[1], Z. Luo[1], K. Shi[1], Y. Tang[1],

K. Huang[1], X. Chen[1], Q. Ye[1], Y. Cao[2], X. Zhou[2,*].

1. Huizhou Power Supply Bureau, Guangdong Power Grid Corporation, Huizhou 516000, China
2. School of Automation, Central South University, Changsha 410083, China

Abstract

To achieve comprehensive energy utilization and economical operation of the system, an optimization operation strategy for a small-scale distillation plant integrated energy system (IES) is proposed in this paper. The system integrates liquid air energy storage sub-system (LAES), thermal energy storage sub-system (TES), and PV modules for the steel mill. The innovation of this work lies in the application of Information Gap Decision Theory (IGDT) to manage uncertainties in waste heat availability, enabling robust energy scheduling across risk-neutral, risk-averse, and risk-seeking scenarios. The paper investigated the impacts of robustness and opportunity radius on the system operating cost and schedule of LAES. The IGDT-based strategy proved most cost-effective, lowering total operating costs to $29,295, outperforming MOGWOA and POA, which yielded $31,748 and $31,657, respectively. The analysis also highlighted that risk awareness critically influences system costs. Specifically, in the risk-averse scenario, increasing the robustness radius from 0.0416 to 0.3279 raised costs from $30,090 to $39,534, while the risk-seeking approach offered a slight reduction in opportunity cost. These results confirm the effectiveness of the IGDT method and underscore its potential in optimizing IES operations under uncertainty.

Keywords: Integrated energy system (IES), Liquid air energy storage (LAES), Waste heat utilization (WHU), Information gap decision theory (IGDT), Scheduling optimization

1. Introduction

With the rapid development of technology and the growth of global population, traditional non-renewable energy sources are becoming insufficient to sustain the ever-increasing energy demands of humanity [1-2]. Integrated energy systems (IES) have become one of the focuses of research [3-4]. Large-scale IES access to multiple renewable energy sources, involving various energy use conversion and storage methods, and the coverage can be achieved across the

* Correspending author. Tel.: +86-18607390157
E-mail addresses: wangyankai@gdhz.csg.cn (K. Wang); caibingzi@gdhz.csg.cn (B. Cai); luozhenhua@gdhz.csg.cn (Z. Luo); shikefan@gdhz.csg.cn (K. Shi); tangye@gdhz.csg.cn (Y. Tang); huangkailong@gdhz.csg.cn (K. Huang); chenxiaoxin@gdhz.csg.cn (X. Chen); yeqiuxiao@gdhz.csg.cn (Q. Ye); caoyuan3116@csu.edu.cn (Y. Cao); zhouxinyao@csu.edu.cn (X. Zhou)

Click here to enter text.

region [5]. A medium-sized IES in a region responsible is only for energy management and dispatch in that region [6]. As far as small-scale IESs are concerned, the steel mill is a subject worthy of research [7]. Energy storage is needed to meet the high electricity demand in industrial parks and to take advantage of time-based pricing in the power grid. Additionally, the steelmaking process generates a significant amount of by-products and waste, which carry valuable excess heat and pressure that can be harnessed to recover and conserve traditional fossil fuel consumption [8]. For waste heat of low and medium grade (below 623.15K) [9], conventional turbines are not economically feasible for electricity generation from medium-grade waste heat at 600K, and the use of organic Rankine cycle for low-grade waste heat raises safety and economic concerns. The failure to recycle such waste heat not only results in energy loss but also contributes to environmental pollution [10].

It is crucial to utilize energy in an environmentally friendly manner to achieve the human sustainable development strategy [11]. As an emerging energy storage technology, liquid air energy storage system (LAES) has significant development potential, and its advantages of high energy storage density and lack of geographical limitation have attracted widespread attention [12]. LAES integrates waste heat resources from steel mills and effectively utilizes them. It also harnesses surplus power from the steel mill's internal grid, charging during periods of low prices and discharging during peak periods. This strategy captures price differentials and enhances the economic benefits for the steel plant.

However, the temperature, generation time, and magnitude steel of waste heat generated in different stages of the steel production process are different. These uncertainties bring many tests for waste heat recovery and utilization stability and safety. For the uncertainties arising from renewable energy sources and multi-energy load forecasting, Mei et al. [13] proposed a multi-scenario operation model based on stochastic optimization. Li et al. [14] proposed a two-stage operation model based on robust optimization and stochastic optimization. And Zhong et al. [15] proposed an operating model based on stochastic optimization considering human psychological preferences. Li et al. [16] proposed an interval optimization model considering multiple uncertainties and a case study of the effects of uncertainty-related factors. Yu et al. [17] presented an enhanced bi-objective optimization approach utilizing triangle split, establishing a bi-objective uncertain optimization framework. This framework aimed to identify the Pareto optimal solution for the operation of community integrated energy systems (CIES) and their economic-environmental management under uncertainties. Liu et al. [18] considered the influence of uncertainties on both supply and demand sides and developed a multi-objective interval optimization model for economy and environmental protection. Nikmehr [19] addressed the problem of dispatching between microgrids and distribution networks, utilizing a robust optimization method to optimize daily operations, using the alternating direction method of multipliers (ADMM) to decentralize daily operations. Zhou et al. [20] built a two-stage robust optimization model under uncertainty based on the C&CG algorithm applying Power to Gas and Hydrogen Compressed Natural Gas in integrated energy systems. Liu et al. [21] proposed a non-cooperative game-theoretic-based collaborative planning method for gas and electricity for integrated electricity-to-gas and grid-based integrated energy systems and a two-stage robust optimization method for wind power and load uncertainty. The optimization methods discussed in the referenced literature primarily address risk neutrality and aversion. However, these approaches may not ensure a comprehensive consideration of both the beneficial and adverse impacts of risk on system operations. Additionally, the operating costs of model optimization could exceed acceptable levels due to the incomplete consideration of risk factors.

Furthermore, Information Gap Decision Theory (IGDT) considers both risk aversion and risk pursuit to provide more decision possibilities for the optimal operation of systems with uncertainty [22]. Yan et al. [23] proposed a quantification method for dynamic risks of variable renewable energy sources, market tariff uncertainties associated with small distributed energy sources integrated into virtual power plants, and applies IGDT to unit commitments to study the impact of tariff uncertainty on virtual power plant operations. Nikoobakht et al. [24] utilized a new fuzzy IGDT to model the uncertainty of wind energy with a continuous-time power demand response plan that facilitates wind power integration. Khazali et al. [25] utilized IGDT to manage uncertainty in wind power and system prices for day-ahead nodal energy market optimization of combined wind/storage units. Bahramara et al. [26] proposed a two-stage stochastic model for day-ahead and real-time dispatch for microgrid operators, and the IGDT approach is used to describe the operator's behavior to address the uncertainty of real-time energy market prices. Wang et al. [27] utilized comprehensive incentives, including time-of-use tariffs and demand response incentive subsidies, to encourage customer participation in demand response. It constructed a two-level stochastic optimal dispatch model for integrated energy systems, considering a stepped carbon trading mechanism and demand response, based on the IGDT. Peng et al. [28] established an integrated energy system comprising multiple energy sources, including heat, electricity, and gas. It adopted a rolling planning cycle spanning fifteen years, divided into five-year phases, and introduces IGDT to address the uncertainty of the electric load. The model's validity is subsequently verified utilizing data from an actual park.

However, most of the IGDT applications in the above literature are for electricity or power loads, and most of the IES compositions in the above references utilizing mostly batteries, without considering the integration of LAES and waste heat utilization. The rational use of waste heat resources can reduce resource waste and the pollution impact of unused waste heat discharged into the atmosphere on the environment. Comprehensive energy utilization in the park helps to improve system operation’s stability and flexibility. Therefore, it is necessary to formulate a reasonable waste heat distribution strategy according to the impact of waste heat uncertainty on the operating cost of enterprises.

The paper can be summarized with the following key contributions:

1) Presented an IES for a steel mill, combining LAES and WHU to enhance energy efficiency.

2) Employed IGDT to develop optimal operation strategies under uncertainty, addressing risk-neutral, risk-averse, and risk-seeking scenarios.

3) Analyzed the impact of robustness and opportunity radius on LAES scheduling, revealing that risk-aware strategies substantially influence system performance.

Nomenclature

		Parameters	
SC	Specific consumption	SP	Specific electric power output
OC	Operation cost	Y	Rated capacity of PV array
η	Storage degradation factor	γ	Storage loss factor
μ	Waste heat utilization factor	ξ	Operation cost factor
f	Derating factor	α_p	Temperature coefficient
eff	Efficiency		
		Variables	
u	The binary variables represent the charge and discharge state of storage system	M	Mass
E	Electric power	H	Heat mass
LAT	Liquid air tank	T_a	Temperature of ambient
T_c	Temperature of PV cell	G_T	Solar irradiance on the PV array
Deg	Degradation of storage system	Eng	Energy storage level
		Acronyms	
IES	Integrated energy system	LAES	Liquid air energy storage system
WHU	Waste heat utilization	TES	Thermal energy storage system
IGDT	Information gap decision theory	PV	PV panels
MILP	Mixed-integer linear programming	MINLP	Mixed-integer nonlinear programming
HS	Heat sale	S	Sale to market
c	Conversion	e	Electricity
o	Operation	max/min	Maximum/minimum value
ra	Risk-averse	rn	Risk neutral
rs	Risk seeking	ch-final	Final charging state of TES
dch-final	Final discharging state of TES	ch/dch	Charging/discharging mode of storage system
wh	Waste heat	exp	Expansion
inv	Inverter	grid	Grid
load	Load	loss	Loss of storage system

The organization of this paper is as follows, Section 1 is the introduction that briefly describes the IGDT utilized below, Section 2 gives the analysis of IES that combines liquid air energy storage for WHU. Section 3 presents the system model. The description of three system optimization operation strategies based on the uncertainty of waste heat mass is provided in Section 4. Section 5 is the experimental analysis to evaluate and validate presented IGDT method. Section 6 gives the conclusion of this paper.

2. Methodology

2.1. IGDT method

IGDT is a non-probabilistic and non-possibilistic method for dealing with models including uncertain input data. The system model is represented by (1), $F(P,\lambda)$ donates the objective function, P and λ indicate the decision variable and the uncertain input data, respectively.

$$\begin{cases} \min F(P,\lambda) \\ s.t. H(P,\lambda)=0 \\ G(P,\lambda)\geq 0 \end{cases} \tag{1}$$

The uncertainty model is expressed by (2)-(3) mathematically, λ expresses the forecasted values of uncertain parameter, α is the uncertainty horizon which means the upper limit value of forecasted input data deviation is $\alpha\lambda$.

$$U(\alpha,\lambda)=\left\{\lambda:\left|\frac{\lambda-\overline{\lambda}}{\overline{\lambda}}\right|\right\}\leq\alpha \tag{2}$$

$$\lambda\in U \tag{3}$$

The risk-averse and risk-seeking strategies are expressed as follows:

In risk-averse IGDT, decision-makers tend to invest higher costs to obtain robust operation, making the system risk-averse and able to withstand greater fluctuations in uncertainty parameters. The risk-averse IGDT-based model of (1) is as below.

$$\begin{cases} \min\alpha(P,\lambda) \\ F(P,\lambda)\leq(1-\kappa)\overline{F} \\ H(P,\lambda)=0 \\ G(P,\lambda)\geq 0 \\ 0\leq\kappa\leq 1 \\ \left|\frac{\lambda-\overline{\lambda}}{\overline{\lambda}}\right|\leq\alpha \end{cases} \tag{4}$$

α donates the robust radius for uncertain parameters, $\overline{F}$ is the forecast cost when the uncertain input data equals the forecasted uncertain data. κ is the cost deviation when considering pursuing robust situations to avoid the risk of the unfavorable uncertain data.

In risk-seeking IGDT, decision-makers tend to profit from favorable deviations to obtain a smaller cost. The risk-seeking IGDT-based model of (1) is as below.

$$\begin{cases} \min \alpha(P,\lambda) \\ F(P,\lambda) \le (1-\chi)\overline{F} \\ H(P,\lambda)=0 \\ G(P,\lambda)\ge 0 \\ 0\le \chi \le 1 \\ \left|\dfrac{\lambda-\overline{\lambda}}{\overline{\lambda}}\right| \le \alpha \end{cases} \tag{5}$$

The opportunity horizon is represented as α, and χ is the cost deviation when considering pursuing positive effects from favorable uncertain data. In fact, the optimal bias of uncertain input data leads to the cost equal to $(1-\chi)\overline{F}$ [29].

2.2. Multi-Objective Gray Wolf Optimization Algorithm (MOGWOA)

The Multi-Objective Grey Wolf Optimizer (MOGWO) [30] is an optimization algorithm inspired by the hunting behavior of grey wolves, primarily designed to solve multi-objective optimization problems. The algorithm mimics the social hierarchy and hunting strategies of grey wolves, which are categorized into four levels: alpha (α), beta (β), delta (δ), and omega (ω). In the algorithm, alpha, beta, and delta represent the three best solutions currently known, while omega represents the remaining candidate solutions. The positions of the wolves are continuously updated through the hunting process to reach the optimal solution $\vec{X}(t+1)$:

Encircling: The distance between a grey wolf and its prey is calculated as follows:

$$\vec{D} = \left|\vec{B}\cdot\overrightarrow{X_p}(t) - \vec{X}(t)\right| \tag{6}$$

Where $\vec{X}(t)$ is the current position vector of the grey wolf, $\overrightarrow{X_p}(t)$ is the position vector of the prey, and $\vec{B}$ is a coefficient vector. The position of the grey wolf is updated utilizing the following equation, where $\vec{A}$ is a coefficient vector:

$$\vec{X}(t+1) = \overrightarrow{X_p}(t) - \vec{A}\cdot\vec{D} \tag{7}$$

The coefficient vectors can be updated utilizing the following equations, where $\vec{a}$ linearly decreases from 2 to 0, and $\overrightarrow{r_1}$ and $\overrightarrow{r_2}$ are random vectors between 0 and 1:

$$\vec{A} = 2\vec{a}\cdot\overrightarrow{r_1} - \vec{a} \tag{8}$$

$$\vec{B} = 2\overrightarrow{r_2} \tag{9}$$

Hunting: The optimal solution is sought by simulating the social leadership and encircling mechanisms of the wolf pack. The positions are updated based on the top three best solutions: alpha, beta, and delta:

$$\begin{cases} \overrightarrow{D_\alpha} = \left|\overrightarrow{B_\alpha}\cdot\overrightarrow{X_{\alpha p}}(t) - \vec{X}(t)\right| \\ \overrightarrow{D_\beta} = \left|\overrightarrow{B_\beta}\cdot\overrightarrow{X_{\beta p}}(t) - \vec{X}(t)\right| \\ \overrightarrow{D_\delta} = \left|\overrightarrow{B_\delta}\cdot\overrightarrow{X_{\delta p}}(t) - \vec{X}(t)\right| \end{cases} \tag{10}$$

The updated positions are then calculated as follows:

$$\begin{cases} \overrightarrow{X_\alpha} = \overrightarrow{X_{\alpha p}}(t) - \overrightarrow{A_\alpha} \cdot \overrightarrow{D_\alpha} \\ \overrightarrow{X_\beta} = \overrightarrow{X_{\beta p}}(t) - \overrightarrow{A_\beta} \cdot \overrightarrow{D_\beta} \\ \overrightarrow{X_\delta} = \overrightarrow{X_{\delta p}}(t) - \overrightarrow{A_\delta} \cdot \overrightarrow{D_\delta} \end{cases} \tag{11}$$

Finally, the new position $\vec{X}(t+1)$ is determined by averaging the positions of these three solutions:

$$\vec{X}(t+1) = \frac{\overrightarrow{X_\alpha} + \overrightarrow{X_\beta} + \overrightarrow{X_\gamma}}{3} \tag{12}$$

In MOGWO, Pareto ranking and crowding distance concepts are employed to handle the characteristics of multi-objective problems, maintaining solution diversity and balancing the optimization of different objectives.

2.3. Pelican Optimization Algorithm (POA)

The Pelican Optimization Algorithm (POA) [31] is an intelligent optimization algorithm inspired by the predatory behaviour of pelicans. POA simulates the behaviour of pelicans during hunting. The algorithm continuously updates the positions of individuals within the population, mimicking the process by which pelicans approach their target (the optimal solution) during hunting. In the algorithm, each pelican represents a candidate solution, and by simulating their behaviour, they gradually converge towards the global optimal solution.

Approaching the Prey: The pelican identifies the location of the prey $\overrightarrow{X_p'}(t)$ and moves towards it, updating its position utilizing the following equation:

$$\overrightarrow{X_1}'(t+1) = \begin{cases} \overrightarrow{X}'(t) + \vec{r_3} \cdot \left(\overrightarrow{X_p'}(t) - I \cdot \overrightarrow{X}'(t)\right), F_p < F_1 \\ \overrightarrow{X}'(t) + \vec{r_3} \cdot \left(\overrightarrow{X}'(t) - \overrightarrow{X_p'}(t)\right), F_p \geq F_1 \end{cases} \tag{13}$$

Where $\overrightarrow{X_1}'(t+1)$ represents the position update during the approach phase, $\overrightarrow{X}'(t)$ is the original position, I is a random integer (either 1 or 2), F_p is the objective function value of the prey, and F_1 is the objective function value of the original position.

Soaring: Once the pelican reaches the vicinity of the prey, it soars over the water surface to capture it. The position is updated as follows:

$$\overrightarrow{X_2}'(t+1) = \overrightarrow{X}'(t) + R \cdot \left(1 - \frac{t}{T_{max}}\right) \cdot \left(2 \cdot \vec{r_4} - 1\right) \cdot \overrightarrow{X}'(t) \tag{14}$$

Where $\overrightarrow{X_2}'(t+1)$ represents the position update during the soaring phase, $\vec{r_3}$ and $\vec{r_4}$ are random vectors between 0 and 1, R is the local search radius, T_{max} is the maximum number of iterations, and t is the current iteration number.

Position Update: The new positions generated in each phase are evaluated and updated as follows:

$$\vec{X}'(t+1)=\begin{cases}\vec{X_i}'(t+1), F_p < F_i \\ \vec{X}'(t), else\end{cases} \tag{15}$$

3. The integrated energy system

In the research, an energy system including electrical and heating hubs integrated LAES to utilize the waste heat as Fig. 1 is utilized, LAES converts electricity during the charging process into liquid air. While discharging, the liquid air is pumped from liquid air tank and superheated to undergo expansion to generate electricity. The thermal energy storage system (TES) is utilized to store and release waste heat recovered during steelmaking process in the form of low-pressure steam.

3.1. LAES constraints

The operation of LAES is subject to constraints (16)-(22) [22, 29].

The energy storage level in LAES at time t is as follows:

$$Eng_{LAES}(t)=Eng_{LAES}(t-1)+E_{ch}(t)-E_{dch}(t)-Eng_{loss}^{LAES}(t) \tag{16}$$

Here, Eng_{LAES} denotes energy storage level in the LAES system. $E_{ch}(t)$ and $E_{dch}(t)$ represent the power stored in the cryogenic tank and the power released to the power hub, respectively. $Eng_{loss}^{LAES}(t)$ corresponds to the energy loss due to the liquid air lost from the cryogenic tank, which can be determined by calculating the storage loss factor of LAES γ_{loss}^{LAES} :

$$Eng_{loss}^{LAES}(t)=\gamma_{loss}^{LAES}Eng_{LAES}(t) \tag{17}$$

The degradation of LAES Deg_{TES} is obtained based on (18), where η_{deg}^{LAES} is the degradation factor of LAES.

$$Deg_{LAES}=\eta_{deg}^{LAES}\sum_t\left(E_{ch}(t)+E_{dch}(t)\right) \tag{18}$$

Furthermore, the following constraints must be satisfied, where E_{ch}^{max} and E_{dch}^{max} represent the maximum power of charging and discharging mode in LAES. $u_{ch,LAES}(t)$ and $u_{dch,LAES}(t)$ are the binary variables represent the charge and discharge state of LAES. Eng_{LAES}^{min} and Eng_{LAES}^{max} denote the maximum and minimum energy storage level in LAES.

$$0 \le E_{ch}(t) \le E_{ch}^{max}u_{ch,LAES}(t) \tag{19}$$

$$0 \le E_{dch}(t) \le E_{dch}^{max}u_{dch,LAES}(t) \tag{20}$$

$$u_{ch,LAES}(t)+u_{dch,LAES}(t)\leq 1 \tag{21}$$

$$Eng_{LAES}^{min}\leq Eng_{LAES}(t)\leq Eng_{LAES}^{max} \tag{22}$$

3.2. TES constraints

The constraints for TES operation are represented as constraints (23)-(31) [22, 29].

The energy storage level in TES at time t is as follows:

$$Eng_{TES}(t)=Eng_{TES}(t-1)+H_{ch-final}(t)-H_{dch}(t)-Eng_{loss}^{TES}(t) \tag{23}$$

Here, Eng_{TES} denotes energy storage level in the TES system. $H_{ch-final}(t)$ represents the thermal energy ultimately stored in the TES. $H_{dch}(t)$ denotes the thermal energy released by the TES Eng_{loss}^{TES} corresponds to the thermal energy loss corresponding to low-pressure steam, which can be determined by calculating the storage loss factor of TES γ_{loss}^{TES} :

$$Eng_{loss}^{TES}(t)=\gamma_{loss}^{TES}Eng_{TES}(t) \tag{24}$$

$H_{ch-final}(t)$ is obtained from thermal storage efficiency of the TES eff_{ch} and the thermal energy stored in the TES $H_{ch}(t)$:

$$H_{ch-final}(t)=eff_{ch}H_{ch}(t) \tag{25}$$

The thermal energy ultimately released in the TES $H_{dch-final}(t)$ is obtained from thermal release efficiency of the TES eff_{dch} and the thermal energy released by the TES $H_{dch}(t)$:

$$H_{dch-final}(t)=eff_{dch}H_{dch}(t) \tag{26}$$

The degradation of TES Deg_{TES} is obtained based on (27), where η_{deg}^{TES} is the degradation factor of TES.

$$Deg_{TES}=\eta_{deg}^{TES}\sum\nolimits_{t}\left(H_{ch}(t)+H_{dch}(t)\right) \tag{27}$$

Furthermore, the following constraints must be satisfied, where H_{ch}^{max} and H_{dch}^{max} represent the maximum thermal energy of charging and discharging mode in TES. $u_{ch,TES}(t)$ and $u_{dch,TES}(t)$ are the binary variables represent the charge and discharge state of TES. Eng_{TES}^{min} and Eng_{TES}^{max} denote the maximum and minimum thermal energy storage level in TES.

$$0\leq H_{ch}(t)\leq H_{ch}^{max}u_{ch,TES}(t) \tag{28}$$

$$0 \le H_{dch}(t) \le H_{dch}^{max} u_{dch,TES}(t) \tag{29}$$

$$u_{ch,TES}(t) + u_{dch,TES}(t) \le 1 \tag{30}$$

$$Eng_{TES}^{min} \le Eng_{TES}(t) \le Eng_{TES}^{max} \tag{31}$$

3.3. WHU constraints

The constraints for WHU are represented as constraints (32)- (36) [33].

$$E_{dch}(t) = SP \times M_{dch}(t) \tag{32}$$

$$E_{ch}(t) = SC \times M_{ch}(t) \tag{33}$$

In this context, SC refers to the specific liquefaction consumption of the LAES, SP indicates the specific electric power output, $M_{ch}(t)$ denotes the mass of liquid air stored after cooling and liquefaction, and $M_{dch}(t)$ represents the mass of liquid air pumped out by the cryogenic pump. The mass of liquid air in the cryogenic tank $LAT_{loss}(t)$ is calculated as follows:

$$LAT(t) = LAT(t-1) + M_{ch}(t) - M_{dch}(t) - LAT_{loss}(t) \tag{34}$$

LAT represents the mass of liquid air stored in the LAES cryogenic tank, while $LAT_{loss}(t)$ refers to the mass of liquid air lost from the cryogenic tank. The $LAT_{loss}(t)$ can be calculated based on the loss ratio γ_{LAT}^{loss} and the initial mass of liquid air in the tank:

$$LAT_{loss}(t) = \gamma_{LAT}^{loss} LAT(t) \tag{35}$$

The numerical relationship between the expanded waste heat and the discharge power is defined as follows:

$$H_{exp}(t) = \mu_{WHU} M_{dch}(t) \tag{36}$$

$H_{exp}(t)$ denotes the mass of waste heat required during the expansion process, while μ_{WHU} represents the proportional coefficient between the mass of waste heat and the electrical energy discharged.

3.4. PV constraints

The operation of PV power generation is subjected to constraints (37)-(40) [35].

The actual temperature of the PV $T_c(t)$ at a specific moment is determined by the actual irradiance $G_T(t)$ and ambient temperature $T_a(t)$:

$$T_c(t) = T_a(t) + G_T(t) \times l \tag{37}$$

Here, l denotes the radiation temperature coefficient. The irradiance and temperature have a direct impact on the output power of the PV.

$$E_p(t) = Y_{PV} \times f_{PV} \times \left(\frac{G_T(t)}{G_{T,STC}} \right) \times \left[1 + \alpha_p \times \left(T_c - T_{c,STC} \right) \right] \tag{38}$$

Specifically, Y_{PV} represents the rated power of the photovoltaic panel measured under standard conditions, f_{PV} is the performance degradation parameter, $G_T(t)$ denotes the actual irradiance received by the panel at a given time, $G_{T,STC}$ represents the irradiance under standard conditions, α_p is the coefficient that modulates the relationship between power and temperature, and $T_{c,STC}$ refers to the ambient temperature.

$$E_{PV}(t) = eff_{inv} \times E_p(t) \tag{39}$$

Final output power of the PV $E_{PV}(t)$ is obtained from conversion efficiency of the PV eff_{dch} and output power of the PV:

$$Deg_{PV} = \eta_{deg}^{PV} \sum\nolimits_t E_{PV}(t) \tag{40}$$

The degradation of PV Deg_{PV} is obtained based on (40), where η_{deg}^{PV} is the degradation factor of PV.

3.5. Balance constraints

The electric and thermal balance constraints are represented as (41) and (42).

$$E_{grid}(t) + E_{PV}(t) + E_{dch}(t) = E_{ch}(t) + E_{load}(t) \tag{41}$$

$$H_{load}(t) + H_{exp}(t) + H_{ch}(t) + H_S(t) = H_{dch-final}(t) + H_{wh}(t) \tag{42}$$

Where $E_{grid}(t)$ represents electricity purchased from the grid, $E_{load}(t)$ represents electricity energy load demand of the plant, $H_{load}(t)$ represents the thermal energy load demand of the plant, $H_S(t)$ represents the thermal energy sold externally by the plant, and $H_{wh}(t)$ represents the waste heat recovered by the plant.

4. Uncertain optimal operation strategies

In this section the model is introduced within three uncertain optimal operation strategies, namely, risk-neutral, risk-averse, and risk-seeking in three subsections.

4.1. Risk-neutral strategy

The constraints of LAES, TES, WHU, PV and electric and thermal balance are presented as (16)-(42). The mixed-integer linear programming (MILP) model for optimal operation in the IES ignoring the uncertainty is characterized by (16)-(42) and (43). In the risk-neutral strategy, the uncertainty of the quality of waste heat is not considered. The EH operation cost is represented as (43). It respectively includes the cost of purchased electricity, the operation cost of LAES, the operation cost of TES, the operation cost of PV panels, the penalty cost of sold purified heat, the degradation cost of LAES, TES and PV.

$$\begin{cases} Cost_e(t) = E_{\mathrm{grid}}(t)\pi_{\mathrm{grid}}(t) \\ Cost_o(t) = \xi_{OC}^{LAES}\left[E_{ch}(t)+E_{\mathrm{dch}}(t)\right] + \xi_{OC}^{TES}\left[H_{ch}(t)+H_{dch}(t)\right] + \xi_{OC}^{PV}E_{PV}(t) \\ Cost_{HS}(t) = \left[\pi_h(t) - \pi_{P_{ur}}\right]H_S(t) \\ Cost_{Deg}(t) = Deg_{LAES} + Deg_{TES} + Deg_{PV} \\ OC = \sum_t Cost_e(t) + Cost_m(t) - Cost_{HS}(t) + Cost_{Deg}(t) \end{cases} \tag{43}$$

4.2. Risk-averse strategy

When the model introduces an IGDT-based risk-averse optimized operating strategy, the model ensures that operating costs do not exceed acceptable levels with maximum fluctuations in the waste heat steam mass. This operating strategy regards fluctuations in the mass of waste heat as an unfavorable factor. The purpose of the strategy is to achieve acceptable target operating costs at the maximum fluctuation, the operating cost of the model should be no higher than the worst-case implementation of the uncertain parameter - $(1-\alpha_h)H_{wh}$.

$$\begin{cases} \alpha = \max\left\{\min OC(\alpha_h)\right\} \\ OC \le OC_{ra} \\ OC_{ra} = (1+\beta)OC_{rn} \\ H_{load}(t) + H_{exp}(t) + H_{ch}(t) + H_S(t) = H_{dch-final}(t) + (1-\alpha_h)H_{wh}(t) \end{cases} \tag{44}$$

subject to constraints (16)-(42), (44).

4.3. Risk-seeking strategy

An IGDT-based risk-seeking optimized operating strategy is introduced, in this strategy, the mass of waste heat is considered as a favorable factor to achieve cost reduction in system operation. This means that the more waste heat mass, the more benefits it will bring to the operation of the system. The purpose of the strategy is to seek the smallest opportunity radius to achieve the target operating cost under the optimal realization of uncertain parameters-$\left(1+\alpha_h\right)H_{wh}$.

$$\begin{cases} \alpha = \min\left\{\min OC\left(\alpha_h\right)\right\} \\ OC \le OC_{rn} \\ OC_{ra} = \left(1-\beta\right)OC_{rn} \\ H_{load}\left(t\right)+H_{exp}\left(t\right)+H_{ch}\left(t\right)+H_S\left(t\right)=H_{dch-final}\left(t\right)+\left(1+\alpha_h\right)H_{wh}\left(t\right) \end{cases} \tag{45}$$

subject to constraints (16)-(42), (45).

5. Experimental Results

In this section, the results of three optimization strategies are presented. A small-scale IES with LAES, TES, PV panels is studied. The presented approach for the studied system is shown in Fig.1, the inputs are the electricity purchased from grid, and the outputs are the steel mill's electricity and heat load. CPLEX solver and DICOPT solver under GAMS optimization software are utilized to solve MILP model and mixed integer nonlinear programming (MINLP) model, respectively [32]. The run time range is 24 hours, and the optimization time unit is 1 hour. Throughout this document, the default units for time, power, and cost are hour (h), MWh and $. The price of electricity and heat, electric and heat load of steel mill, the forecasts of PV power and the mass of waste heat steam are shown in Fig. A1 in the Appendix A1. Parameter values referenced from the literature [33-35] and shown in Table A1 in the Appendix A2.

5.1. Risk-neutral strategy of the system

The risk-neutral results are gained when considering the actual waste heat mass has the same value as the forecasted. Without considering the uncertainty of waste heat, the operation cost of integrated system is $29,295 including $29,720 as the cost of purchasing electricity, $258 as the operation cost, $16 as the cost of component degradations and $699 as the penalty for sold heat.

The results of comparing the deterministic operating costs with and without LAES are shown in Table 1. In terms of total cost, utilizing LAES results in a $1,770 cost reduction compared to not utilizing it. Without LAES, the operation cost and degradation cost are caused by the PV panels. At the same time, not utilizing LAES means no waste heat is recovered for use, so the heat sale penalty is 0. Comparing the costs, although the use of LAES will bring more operation costs and deterioration costs, the value is not very large, the cost of purchasing power compared to not utilizing LAES has decreased $1,330, and the total operating cost comparison is still advantageous. This shows that the addition of LAES benefits the economic operation of the system.

The operation states of electrical and heating hubs are shown in Fig. 2. The area above the x-axis indicates the power or mass flowing into the corresponding hub, while the area below the x-axis indicates the outflow value. From Fig. 2(a), it can be seen that most of the steel mill's electricity load is supplied by the electricity market, LAES charges in the valley tariff and discharges a portion of the electricity load in the peak tariff, reducing the steel mill's electricity purchase at the peak tariff through valley power peak use. The power of LAES reaches the maximum during the whole charging period while the discharging power does not its maximum in 20:00-21:00. The reason for this situation is that the charging of LAES is not associated with heat, while the discharging process requires the use of waste heat, which is constrained by the thermal balance.

In Fig. 2(b) the heat load of the steel mill is fully borne by the waste heat. In the initial hours of TES operation, to maintain heat balance during the peak tariff period of LAES discharge, the surplus waste heat, after fulfilling the heating load, is directly charged into the TES if it is less than the capacity. Should the residual waste heat exceed the maximum permissible heat discharge, heat sales are executed prior to heat charging. If it falls below this threshold, heat sales and charging volumes are adjusted for economic efficiency. Subsequently, during LAES discharge intervals, TES discharges to maximize heat sales post meeting the heating load and expansion heat requirements. During other intervals, heat sales are maximized or managed according to economic considerations.

With the aim of confirming the effectiveness of the IGDT method for dispatching the IES utilized in the study, the Multi-Objective Gray Wolf Optimization Algorithm (MOGWOA) and the Pelican Optimization Algorithm (POA) were utilized to obtain comparative dispatching results. Table 2 shows the total system operating cost and the components under the three scheduling methods, compared with the other two methods, the IGDT method has more advantages. The specific performance is that the electricity purchase cost of the IGDT method is much smaller, which means that the degree of LAES participation under the IGDT method is higher, as can be seen from the value of operation costs. At the same time, from the perspective of heat sale penalty, the IGDT method still achieves better performance than the remaining two methods. This means that the participation of TES under the IGDT method is also more active.

The operating status of LAES and TES is more specifically presented in Fig. 3(a)-(c). POA gets a smaller electricity purchase cost because of less use of LAES for charging, and less use of TES to get a smaller heat sale penalty. MOGWOA utilizes more LAES to charge and purchase electricity at a higher cost, and utilizes more TES to get greater heat sales penalty. The operating status of LAES and TES is verified from the operation cost, and then the total cost obtained by the last two optimization methods is not much different.

The detailed dispatch schemes obtained by the three methods are shown in Fig. 3(b)-(c). The total electricity purchased from the grid by the IGDT method is 404.08MWH, while the MOGWOA method and the POA method are 406.99MWH and 401.1MWH respectively. In terms of the total purchased electricity, the three methods are not much different, but the IGDT method is more effective in terms of electricity purchase cost. It can be seen from Fig. 3(a)-(c) that the IGDT method has more valley electricity prices purchasing and less peak electricity prices purchasing than other methods. Correspondingly, the operation of LAES and TES is also affected. The participation of LAES and TES in scheduling, as assessed by the IGDT method, demonstrates greater intensity compared to other approaches. Specifically, during peak electricity price periods, the variations in capacity for both LAES and TES are more pronounced under the IGDT method than under alternative methods. Figs. 3(b) and 3(c) illustrate that the maximum capacities achieved by LAES and TES under the IGDT method substantially exceed those observed with the other methods. Similarly, the peak charging and discharging powers for LAES and the highest thermal inputs and outputs for TES also reach higher levels under the IGDT method.

5.2. Risk-averse strategy of the system

In this subsection, a risk-averse strategy is introduced to the system based on IGDT, considering waste heat mass as an unfavorable factor. As a robust decision strategy, the primary goal is to ensure that the system's operating cost is below an acceptable value under adverse fluctuations in waste heat. Compared to minimizing the operating cost when no risk is considered, the risk-averse scenario maximizes the robustness radius of the uncertain parameter waste heat mass. The relationship between robust operating cost and robust radius is shown in Fig. 3(d); from the figure, it can be seen that the uncertainty of waste heat is an unfavorable factor; as the uncertainty radius becomes larger, the trend of increasing robust operating cost is fast, the reason for this is the large base of the waste heat mass. As the available waste heat diminishes, to preserve thermal equilibrium, there is a reduction in the expansion heat associated with LAES power generation, leading to a decrease in LAES discharge power. Consequently, this necessitates an increase in electricity purchase costs when waste heat falls to levels insufficient to sustain LAES discharge, while the robust radius either remains stable or alters minimally.

Combining Figs. 3(e) and 3(f) validates the observations from Figure 3(a). As the robust radius expands, the charging and discharging dynamics of the LAES shift from balanced levels to a dominance of charging power over discharging power. This progression culminates in a scenario where only minimal power charging occurs, eliminating discharging activities altogether and subsequently elevating robust operating costs. Concurrently, the pattern of grid electricity purchases adjusts, characterized by reduced power acquisitions during off-peak hours from 6:00 to 8:00 and escalated purchases during peak times at 11:00 to 13:00 and 19:00 to 20:00. These adjustments are primarily responsible for the rise in operating costs, stemming from decreased grid purchases during low tariff periods and increased acquisitions during high tariff intervals.

A more direct comparison of the data can be observed in Table 3. In the cases of α =0.0416 and α =0.1698, LAES undergoes both charging and discharging cycles. From the charging and discharging power values, it is evident that LAES is not fully discharged as the robust radius increases. Furthermore, both the charging and discharging power of LAES rise, leading to an increased difference between the total power charged and the total power discharged. As a result, the total grid electricity purchase at α =0.1698 only increases by 1.25 MW compared to α =0.0416. The robust costs for α =0.0416 and α =0.1698 are $30,090 and $30,163, respectively, indicating that the difference between the robust cost values at these two radii is minimal.

α =0.2148 and α =0.3279 are cases of LAES without discharging. The difference is that in the case of α =0.2148, only the minimum capacity is maintained, while in the case of α =0.3279, the charging power reaches 5MW. Considering all electricity purchased from the grid, the electricity purchased for α =0.3279 increases by 4.2441MW compared to α =0.2148, but the robust costs for two cases are $30,603 and $39,534 respectively, which is a very large difference. The reason is that the robust cost is only the upper bound of the system operating cost, and setting the robust cost does not mean that the actual optimized operating cost of the system is that value.

5.3. Risk-seeking strategy of the system

In this subsection, the role of the decision-maker is that of an optimistic risk chaser. The objective of this model is to find a minimum opportunity radius that allows it to be run at a certain set of acceptable values. The favorable impact of waste heat uncertainty will be exploited so that decision makers benefit from the favorable deviation and thus get the set target operating cost or the opportunity cost.

Fig. 3(g) illustrates the relationship between the opportunity radius and the opportunity operation cost, which decreases as the opportunity radius increases. The reduction of opportunity operating cost mainly comes from the valley-to-peak use of LAES and the heat sale penalty. The composition of the total cost indicates that waste heat influences the overall cost by affecting the operation of LAES and the profit from external heat sales. The increase in the quality of waste heat primarily impacts LAES operation by extending the discharge time, thereby enhancing the effectiveness of peak load shifting. This is reflected in the total discharge power during peak tariff periods. As shown in Fig. 3(h), with the increase in the opportunity radius, the discharge hours during peak tariff periods also increase sequentially to 3, 4, 6, and 7 hours. Simultaneously, the charging hours also increase in the order of 5, 6, 9, and 11 hours. However, due to the constraints of peak tariff periods and the maximum discharge power, the increase in waste heat within the opportunity radius has a limited effect on boosting the total discharge power of LAES. Similarly, the penalty for heat sales is also limited by the maximum allowable heat sale volume.

By comparing Fig. 3(h) and Fig. 3(i), it can be observed that as the opportunity radius increases, LAES increases its charging power during off-peak electricity prices and its discharging power during peak electricity prices. Consequently, the electricity purchased by steel mills during off-peak periods also increases with the rise in the opportunity radius, specifically at 00:00-02:00, 03:00-05:00, and 13:00-16:00. Conversely, the electricity purchased during peak periods decreases as the opportunity radius increases, particularly between 17:00 and 21:00. From Fig. 3(i), it is evident that the difference in grid electricity purchases across various opportunity radii is not substantial. This is primarily because the most significant factor influencing this difference is the operating condition of LAES. The charging and discharging power of LAES varies between 0 and 5 MW. For much of the time, LAES operates consistently across different opportunity radii. Additionally, the variation in charging and discharging power during peak and off-peak hours remains within the 0-5 MW range. Therefore, the fluctuations in grid electricity purchases are similarly affected by these corresponding changes.

To make LAES better for peak use in the valley, it is necessary to increase the waste heat mass at the peak tariff moment. It is clear that the increase in the opportunity radius has a limited effect on the increase in the waste heat mass at the peak tariff moment. In the range of thermal equilibrium, it is difficult to achieve a significant increase in LAES discharge power by increasing the opportunity radius, so the opportunity cost reduction is small.

From the data in Table 4, the relationship between LAES operating state, grid electricity purchase and opportunity radius can be seen more intuitively. As the radius of opportunity increases, the charging power of LAES increases in the 1-5, 14-16 time period. The larger the radius of opportunity, the greater the charging power until the maximum charging power, and the discharge power increases in the 17-21 time period. The larger the radius of opportunity, the greater the discharge power, but limited by the constraints of thermal balance, even at the maximum radius of opportunity, the full maximum power discharge before the peak electricity price period. The corresponding power grid purchases also change with the operating state of LAES, the charging power increases, the electricity purchase increases, and the discharge power increases and the electricity purchase decreases. During other periods of time that are not discussed, the operating status of LAES and electricity purchased from the grid were not affected by the radius of opportunity. The difference between total LAES charging and total LAES also discharging increases. However, because the charging time is mostly in the valley tariff period, the cost of valley power peak use reduction is greater than the cost of electricity purchase increase, so the opportunity cost is decreasing, but the LAES output power is limited compared to the electric load, and the cost reduction effect is limited.

6. Conclusion

This paper, focuses on the integration of LAES and WHU systems in a steel plant, utilizing energy dispatch strategies to optimize system operation and enhance its economic performance. Waste heat can be utilized here to increase the temperature of the liquid air when it enters the turbine, thus increasing the power generation. Based on IGDT, energy scheduling is done from risk-neutral, risk-averse, and risk-seeking strategies considering waste heat mass's uncertainty. In the risk-neutral strategy, IGDT, MOGWOA and POA are utilized to optimize the system after running the total system operating cost of \$29,295, \$31,748 and \$31,657, respectively, the total cost obtained under IGDT optimization has a significant advantage, and the effectiveness of the IGDT optimization method is verified.

In the risk-averse strategy, as the robustness radius increases from 0.0416 to 0.3279, the corresponding robustness cost also increases from \$30,090 to \$39,534, mainly because the mass of waste heat is considered an unfavorable factor by the operator. During system operation, efforts are made to minimize the impact of waste heat mass, resulting in a reduction of waste heat usage. This leads to a decrease in both the power and frequency of LAES discharges, consequently raising electricity purchase costs. Simultaneously, penalties associated with heat sales diminish, while the costs associated with maintaining robustness escalate. In the risk-chasing strategy, the operator considers the waste heat quality as a profitable factor. As the opportunity radius increases, the quality of waste heat improves, leading to more frequent and powerful LAES discharges utilizing waste heat. This continues until all discharge periods reach the maximum discharge power. Consequently, the cost of power purchases decreases while the gains from heat sales increase, causing the overall opportunity cost to decrease. However, this decrease is limited to a few hundred dollars. This limitation arises because LAES output is constrained by its maximum discharge power, restricted by peak and off-peak tariffs, and further limited by heat balance constraints. It is anticipated that future research, focusing on improving LAES performance and waste heat recovery technology, could significantly enhance the economic viability and effectiveness of the IES discussed in this paper.

Acknowledgements

This work is supported by National Natural Science Foundation (NNSF) of China under Grant 62103443 and

61973322, by Hunan Natural Science Foundation under Grant 2022JJ40630 and the Royal Society, UK [IES\R3\213189].

References

1. Wu X., Liao B., Su Y., et al. "Multi-objective and multi-algorithm operation optimization of integrated energy system considering ground source energy and solar energy", *International Journal of Electrical Power & Energy Systems* 2023, 144: 108529.
2. Wang L., Dong H., Lin J., et al. "Multi-objective optimal scheduling model with IGDT method of integrated energy system considering ladder-type carbon trading mechanism", *International Journal of Electrical Power & Energy Systems* 2022, 143: 108386.
3. Hu J., Wang Y., Dong L. "Low carbon-oriented planning of shared energy storage station for multiple integrated energy systems considering energy-carbon flow and carbon emission reduction", *Energy* 2024, 290: 130139.
4. Shi J., Teh J. "Load forecasting for regional integrated energy system based on complementary ensemble empirical mode decomposition and multi-model fusion", *Applied Energy* 2024, 353: 122146.
5. Gan W., Yan M., Yao W., et al. "Decentralized computation method for robust operation of multi-area joint regional-district integrated energy systems with uncertain wind power", *Applied Energy* 2021, 298: 117280.
6. Liu H., Xiang C., Xu Z., et al. "Synergetic planning method for energy stations, pipeline networks, and demand response", *Sustainable Energy Technologies and Assessments* 2023, 57: 103207.
7. Li P., Wang Z., Liu H., et al. "Bi-level optimal configuration strategy of community integrated energy system with coordinated planning and operation", *Energy* 2021, 236: 121539.
8. Andrade C., Desport L., Selosse S. "Net-negative emission opportunities for the iron and steel industry on a global scale", *Applied Energy* 2024, 358: 122566.
9. Zhang M., Shi L., Hu P., et al. "Carnot battery system integrated with low-grade waste heat recovery: Toward high energy storage efficiency", *Journal of Energy Storage* 2023, 57: 106234.
10. Zhang J., Liu Z. "Low carbon economic scheduling model for a park integrated energy system considering integrated demand response, ladder-type carbon trading and fine utilization of hydrogen", *Energy*, 2024, 290: 130311.
11. Karaca A. E., Dincer I., Nitefor M. "Development of an integrated solar and wind driven energy system for desalination and power generation", *Sustainable energy technologies and assessments*, 2022, 52: 102249.
12. Kandezi M. S., Naeenian S. M. M. "Investigation of an efficient and green system based on liquid air energy storage (LAES) for district cooling and peak shaving: Energy and exergy analyses", *Sustainable Energy Technologies and Assessments*, 2021, 47: 101396.
13. Mei F., Zhang J., Lu J., et al. "Stochastic optimal operation model for a distributed integrated energy system based on multiple-scenario simulations", *Energy*, 2021, 219: 119629.
14. Li P., Wang Z., Wang J., et al. "Two-stage optimal operation of integrated energy system considering multiple uncertainties and integrated demand response", *Energy*, 2021, 225: 120256.
15. Zhong J., Li Y., Cao Y., et al. "Stochastic optimization of integrated energy system considering network dynamic characteristics and psychological preference", *Journal of Cleaner Production*, 2020, 275: 122992.
16. Li Y., Wang K., Gao B., et al. "Interval optimization based operational strategy of integrated energy system under renewable energy resources and loads uncertainties", *International Journal of Energy Research*, 2021, 45(2): 3142-3156.
17. Yu H., Tian W., Yan J., et al. "Improved triangle splitting based bi-objective optimization for community integrated energy systems with correlated uncertainties", *Sustainable Energy Technologies and Assessments*, 2022, 49: 101682.
18. Liu H., Tian S., Wang X., et al. "Optimal planning design of a district-level integrated energy system considering the impacts of multi-dimensional uncertainties: A multi-objective interval optimization method", *IEEE Access*, 2021, 9: 26278-26289.
19. Nikmehr N. "Distributed robust operational optimization of networked microgrids embedded interconnected energy hubs", *Energy*, 2020, 199: 117440.

20. Zhou S., Sun K., Wu Z., et al. “Optimized operation method of small and medium-sized integrated energy system for P2G equipment under strong uncertainty”, *Energy*, 2020, 199: 117269.
21. Liu Y., Liu T. “Research on system planning of gas-power integrated system based on improved two-stage robust optimization and non-cooperative game method”, *IEEE Access*, 2021, 9: 79169-79181.
22. Yan C., Wang C., Hu Y., et al. “Optimal operation strategies of multi-energy systems integrated with liquid air energy storage using information gap decision theory”, *International Journal of Electrical Power & Energy Systems*, 2021, 132: 107078.
23. Yan X., Gao C., Song M., et al. “An IGDT-based day-ahead co-optimization of energy and reserve in a VPP considering multiple uncertainties”, *IEEE Transactions on Industry applications*, 2022, 58(3): 4037-4049.
24. Nikoobakht A., Aghaei J., Shafie-Khah M., et al. “Continuous-time co-operation of integrated electricity and natural gas systems with responsive demands under wind power generation uncertainty”, *IEEE Transactions on Smart Grid*, 2020, 11(4): 3156-3170.
25. Khazali A., Rezaei N., Su W., et al. “Risk-aware bilevel optimal offering strategy of a joint wind/storage unit based on information gap decision theory”, *IEEE Systems Journal*, 2020, 15(2): 1939-1949.
26. Bahramara S., Sheikhahmadi P., Chicco G., et al. “Modeling the microgrid operator participation in day-ahead energy and reserve markets considering stochastic decisions in the real-time market”, *IEEE Transactions on Industry Applications*, 2022, 58(5): 5747-5762.
27. Wang L., Lin J., Dong H., et al. “Optimal dispatch of integrated energy system considering ladder-type carbon trading”, *Journal of System Simulation*, 2022, 34(7): 1393-1404.
28. Peng Q., Wang X., Shuai X., et al. “Planning of Integrated Energy System Based on Information Gap Decision Theory”, *2021 6th International Conference on Power and Renewable Energy (ICPRE). IEEE*, 2021: 1489-1494.
29. Jordehi A. R., Javadi M. S., Shafie-khah M., et al. “Information gap decision theory (IGDT)-based robust scheduling of combined cooling, heat and power energy hubs”, *Energy*, 2021, 231: 120918.
30. Yousri D., Thanikanti S. B., Balasubramanian K., et al. “Multi-objective grey wolf optimizer for optimal design of switching matrix for shaded PV array dynamic reconfiguration”, *IEEE Access*, 2020, 8: 159931-159946
31. SeyedGarmroudi S. D., Kayakutlu G., Kayalica M. O., et al. “Improved Pelican optimization algorithm for solving load dispatch problems”, *Energy*, 2024, 289: 129811.
32. “GAMS User’s Guide.” https://www.gams.com/latest/docs/UG_MAIN.html (accessed Aug. 14, 2024).
33. Tafone A., Romagnoli A., Borri E., et al. “New parametric performance maps for a novel sizing and selection methodology of a Liquid Air Energy Storage system”, *Applied energy*, 2019, 250: 1641-1656.
34. “Aspen HYSYS V11.” https://www.aspentech.com/en (accessed Aug. 14, 2024).
35. “HOMER Help Manual.” Accessed: Aug. 14, 2024. [Online]. Available: https://www.homerenergy.com/pdf/HOMERHelpManual.pdf

Figures and tables

Caption list

Fig. 1. Scheme of IES.

Fig. 2. (a) The operation strategy of electric hub; (b) The operation strategy of heating hub.

Fig. 3. (a) Purchased power from grid of three methods; (b)Stored power of LAES of three methods; (c) Stored mass of TES of three methods; (d) Robustness radius; (e) LAES states under different robustness radius; (f) Purchased electricity under different robustness radius; (g) Opportunity radius; (h) LAES states under different opportunity radius; (i)Purchased electricity under different opportunity radius.

Table 1. Operation cost comparison between with and without LAES.

Table 2. IGDT, MOGWOA and POA cost comparison.

Table 3. Comparison of LAES states and purchased electricity for risk-averse decision-making considering waste heat uncertainty.

Table 4. Comparison of LAES states and purchased electricity for risk-seeking decision-making considering waste heat uncertainty.

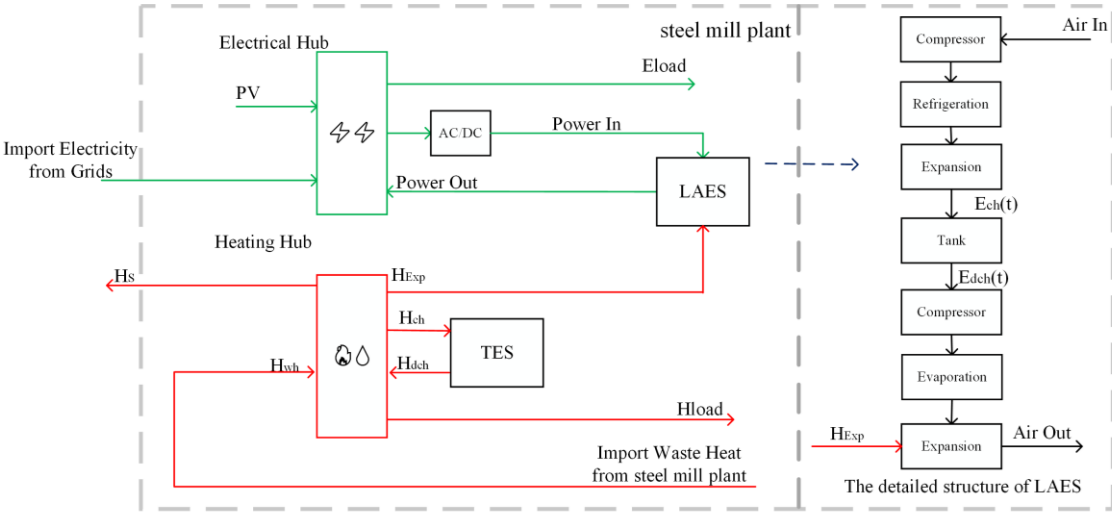

Fig. 1. Scheme of IES.

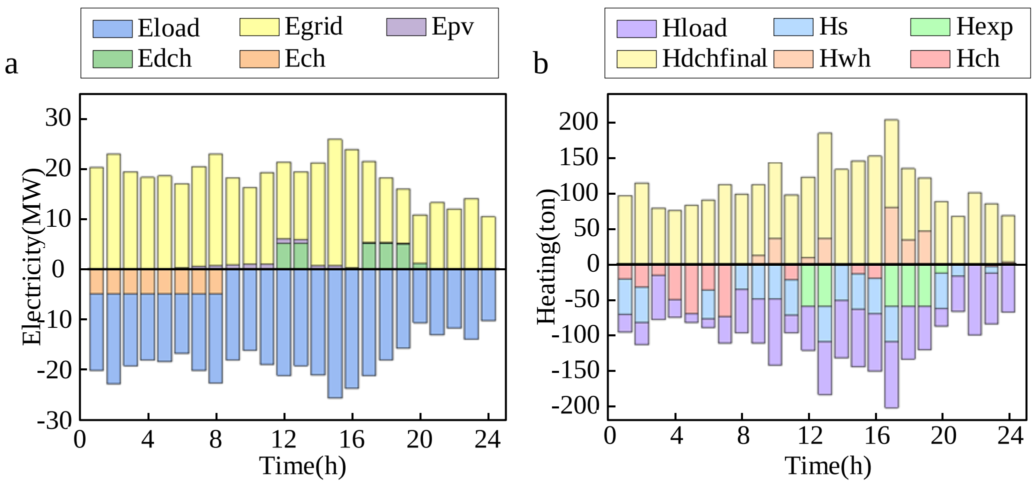

Fig. 2. (a) The operation strategy of electric hub; (b) The operation strategy of heating hub.

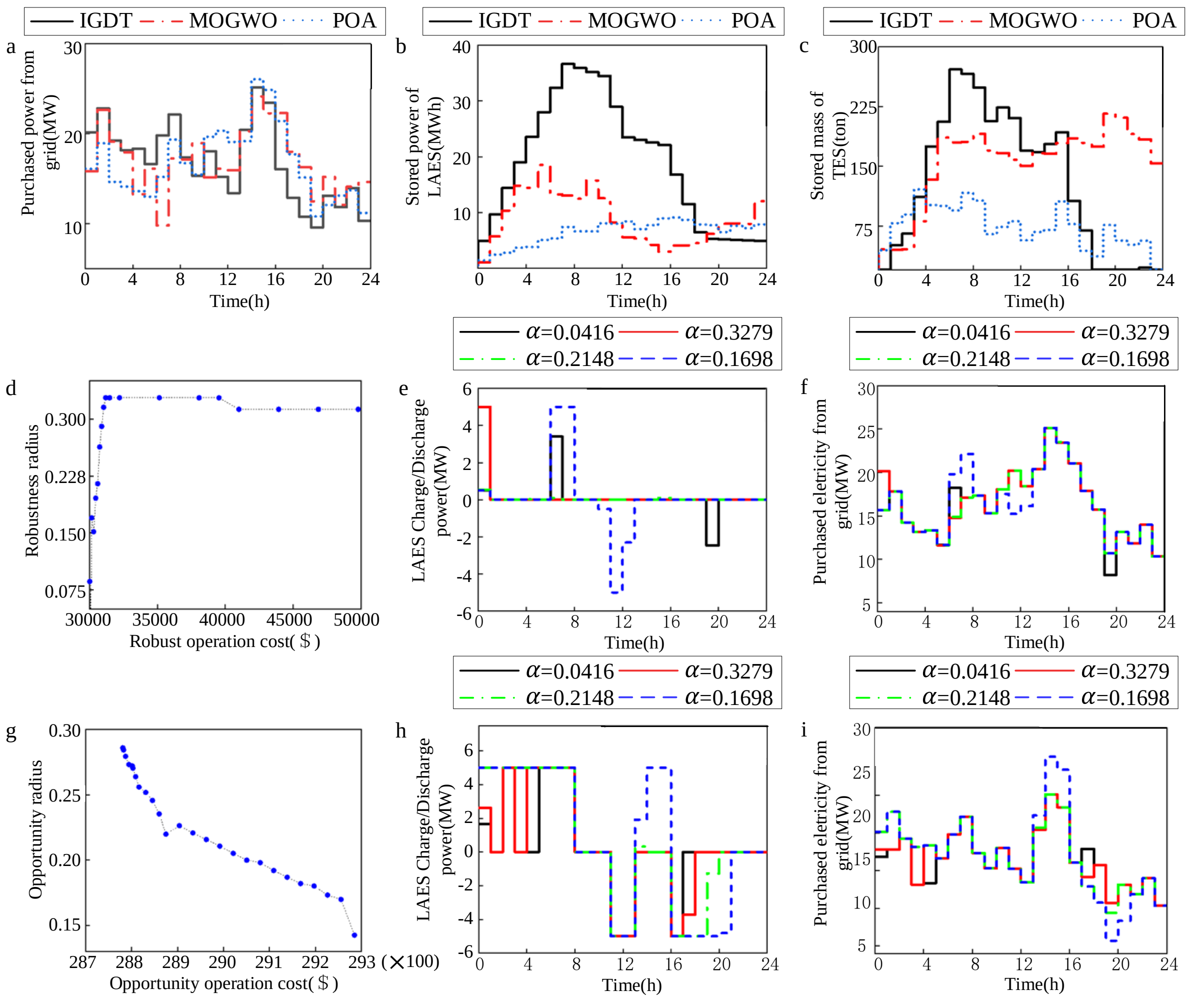

Fig. 3. (a) Purchased power from grid of three methods; (b)Stored power of LAES of three methods; (c) Stored mass of TES of three methods; (d) Robustness radius; (e) LAES states under different robustness radius; (f) Purchased electricity under different robustness radius; (g) Opportunity radius; (h) LAES states under different opportunity radius; (i)Purchased electricity under different opportunity radius.

Table 1. Operation cost comparison between with and without LAES.

	LAES	Without LAES
Electricity purchase ($)	29,720	31,051
Operation ($)	258	8
Degradation ($)	16	6
Penalty for sold heat ($)	699	0
SUM ($)	29295	31065

Table 2. IGDT, MOGWOA and POA cost comparison.

	IGDT	MOGWOA	POA
Electricity purchase ($)	29,720	32,120	31,896
Operation ($)	258	201	81
Degradation ($)	16	14	9
Penalty for sold heat ($)	699	587	330
SUM ($)	29,295	31,748	31,657

Table 3. Comparison of LAES states and purchased electricity for risk-averse decision-making considering waste heat uncertainty.

Hour	LAES states	purchased electricity	LAES states	purchased electricity	LAES states	purchased electricity	LAES states	purchased electricity
	α =0.0416		α =0.1698		α =0.2148		α =0.3279	
1	0.51	15.65833	0.51	15.65833	0.5305	15.67893	5	20.14833
2	0.01	17.81652	0.01	17.81652	0	17.80652	0	17.80652
3	0.01	14.25048	0.01	14.25048	0	14.24048	0	14.24048
4	0.01	13.15059	0.01	13.15059	0.01	13.15059	0	13.14059
5	0.01	13.34254	0.01	13.34254	0.0202	13.35274	0	13.33254
6	0.01	11.63056	0.01	11.63056	0	11.62056	0	11.62056
7	3.40791	18.20313	5	19.79522	0.09755	14.89277	0	14.79522
8	0	17.12083	5	22.12083	0	17.12083	0	17.12083
9	0	17.33684	0	17.33684	0	17.33684	0	17.33684
10	0	15.30477	0	15.30477	0	15.30477	0	15.30477
11	0	18.0403	-0.50503	17.53527	0	18.0403	0	18.0403
12	0	20.22849	-5	15.22849	0	20.22849	0	20.22849
13	0	18.42135	-2.30509	16.11625	0	18.42135	0	18.42135
14	0	20.40039	0	20.40039	0.09755	20.40039	0	20.40039
15	0	25.12903	0	25.12903	0	25.12903	0	25.12903
16	0	23.40839	0	23.40839	0	23.50594	0	23.40839
17	0	21.05783	0	21.05783	0	21.05783	0	21.05783
18	0	17.88469	0	17.88469	0	17.88469	0	17.88469
19	0	15.74109	0	15.74109	0	15.74109	0	15.74109
20	-2.4689	8.20806	0	10.67696	0	10.67696	0	10.67696
21	0	13.13848	0	13.13848	0	13.13848	0	13.13848
22	0	11.83677	0	11.83677	0	11.83677	0	11.83677
23	0	13.97878	0	13.97878	0	13.97878	0	13.97878
24	0	10.32431	0	10.32431	0	10.32431	0	10.32431

Table 4. Comparison of LAES states and purchased electricity for risk-seeking decision-making considering waste heat uncertainty.

Hour	LAES states	purchased electricity	LAES states	purchased electricity	LAES states	purchased electricity	LAES states	purchased electricity
	α =0.1424		α=0.1919		α =0.2353		α =0.2860	
1	1.66809	16.81641	2.63784	17.78616	5	20.14833	5	20.14833
2	0	17.80652	0	17.80652	5	22.80652	5	22.80652
3	5	19.24048	5	19.24048	5	19.24048	5	19.24048
4	0	13.14059	0	13.14059	5	18.1406	5	18.1406
5	0	13.33254	5	18.33254	5	18.33254	5	18.33254
6	5	16.62056	5	16.62056	5	16.62056	5	16.62056
7	5	19.79522	5	19.79522	5	19.79522	5	19.79522
8	5	22.12083	5	22.12083	5	22.12083	5	22.12083
9	0	17.33684	0	17.33684	0	17.33684	0	17.33684
10	0	15.30477	0	15.30477	0	15.30477	0	15.30477
11	0	18.0403	0	18.0403	0	18.0403	0	18.0403
12	-5	15.22849	-5	15.22849	-5	15.22849	-5	15.22849
13	-5	13.42135	-5	13.42135	-5	13.42135	-5	13.42135
14	0	20.40039	0	20.40039	0.32603	20.72642	1.92321	22.3236
15	0	25.12903	0	25.12903	0	25.12903	5	30.12903
16	0	23.40839	0	23.40839	0	23.40839	5	28.40839
17	-5	16.05783	-5	16.05783	-5	16.05783	-5	16.05783
18	0	17.88469	-3.72485	14.15984	-5	12.88469	-5	12.88469
19	0	15.74109	0	15.74109	-5	10.74109	-5	10.74109
20	0	10.67696	0	10.67696	-1.27189	9.40507	-5	5.67696
21	0	13.13848	0	13.13848	0	13.13848	-4.81097	8.32752
22	0	11.83677	0	11.83677	0	11.83677	0	11.83677
23	0	13.97878	0	13.97878	0	13.97878	0	13.97878
24	0	10.32431	0	10.32431	0	10.32431	0	10.32431

Appendix A

The price of electricity and heat, electric and heat load of steel mill, the forecasts of PV power and the mass of waste heat steam are shown in Fig. A1 in the Appendix A.1. Parameter values referenced from the literature [32-34] and shown in Table A1 in the Appendix A.2.

A.1. Price and load

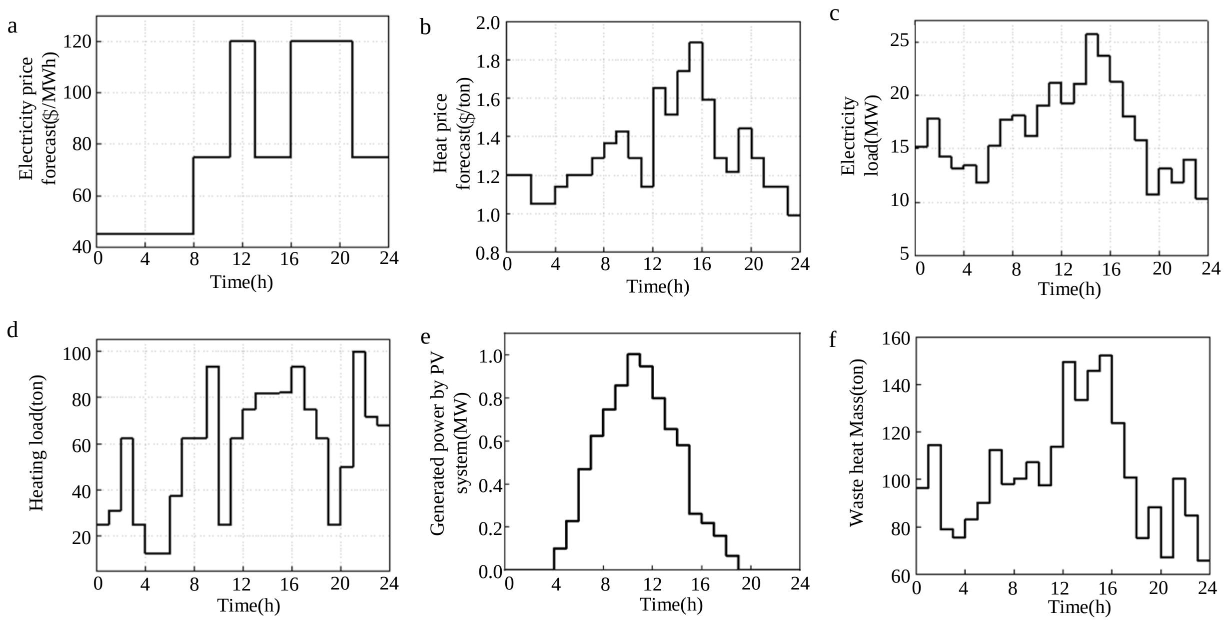

Fig. A1. (a) Electricity price; (b)Heating price; (c) Electricity load; (d) Heating load; (e) The generated power of PV system; (f) Waste heat mass.

A.2. Parameter values

Table A1. Parameters referenced.

Parameter	Value	Parameter	Value
SC	168 KW/ton	η_{deg}^{LAES}	1.515$/MW
SP	0.012 KW/ton	η_{deg}^{TES}	0.0003787$/ton
γ_{loss}^{LAES}	0.02	η_{deg}^{PV}	5.575$/MW
γ_{loss}^{TES}	0.02	ξ_{OC}^{LAES}	37.878$/MW
γ_{loss}^{LAT}	0.02	ξ_{OC}^{TES}	0.378$/ton
μ_{WHU}	1.654 ton/KW	ξ_{OC}^{PV}	1.060$/MW
$\pi_{P_{ur}}$	0.3787$/ton		

Biographies

Kaiyan Wang is a dedicated professional at the Huizhou Bureau of China Southern Power Grid, where he plays a significant role in advancing the development and integration of new power systems. He earned his bachelor's degree in Electrical Engineering from North China Electric Power University, a prestigious institution renowned for cultivating talent in the energy sector. His expertise lies in exploring innovative solutions and technologies to enhance the reliability, efficiency, and sustainability of modern power grids.

Bingzi Cai is an accomplished engineer at the Huizhou Bureau of China Southern Power Grid, specializing in the research and implementation of new power systems. She graduated with a bachelor's degree in Electrical Engineering from North China Electric Power University, which has a strong reputation for its rigorous academic programs in energy engineering. Her work focuses on addressing the challenges of modern power systems, including renewable energy integration and system stability.

Zhenhua Luo is a highly skilled professional at the Huizhou Bureau of China Southern Power Grid, where he contributes to critical advancements in power system fault diagnosis and energy storage solutions. His expertise lies in developing robust diagnostic techniques to ensure system reliability and integrating advanced energy storage technologies to support the evolving needs of the power grid. His work aims to bolster the efficiency and resilience of energy infrastructure.

Kefan Shi serves as a key member of the Huizhou Bureau of China Southern Power Grid, where he is committed to driving innovations in new power systems. With a focus on enhancing the adaptability and sustainability of power grids, he works on integrating cutting-edge technologies and methodologies to address the demands of modern energy systems. His contributions are pivotal to the organization's mission to achieve energy transition and modernization.

Ye Tang is an expert in energy system scheduling optimization at the Huizhou Bureau of China Southern Power Grid. His work revolves around developing and applying advanced optimization strategies to improve the efficiency, stability, and flexibility of energy systems. By leveraging state-of-the-art techniques, he contributes to creating solutions that support renewable energy integration and the long-term sustainability of the power grid.

Kailong Huang is a proficient engineer specializing in energy system scheduling optimization at the Huizhou Bureau of China Southern Power Grid. His work focuses on formulating innovative optimization strategies to enhance the operational performance and reliability of modern energy systems. With a strong commitment to addressing the challenges of energy transition, he plays a critical role in ensuring the grid's efficiency and adaptability.

Xiaoxin Chen is a dedicated professional at the Huizhou Bureau of China Southern Power Grid, where he specializes in scheduling optimization of energy systems. His expertise lies in designing and implementing advanced scheduling methodologies that optimize the operation of power systems. His work is instrumental in promoting the integration of renewable energy sources and improving the overall efficiency and resilience of the grid.

Qiuxiao Ye is an accomplished engineer at the Huizhou Bureau of China Southern Power Grid, focusing on the scheduling optimization of energy systems. His work involves the application of cutting-edge optimization techniques to enhance the performance and sustainability of power systems. By addressing complex challenges in energy scheduling, he contributes to the modernization and decarbonization of the power grid.

Yuan Cao is an associate professor at the School of Automation, Central South University, with extensive expertise in energy storage systems and energy conversion. He earned both his BSc and MSc in Electrical Engineering from Central South University and later pursued his PhD in Electrical Engineering at The University of Alabama, where he gained deep insights into advanced energy technologies. His research focuses on improving the performance and reliability of energy storage systems, with an emphasis on their integration into modern power grids and renewable energy applications.

Xinyao Zhou is a master's student at the School of Automation, Central South University, specializing in the scheduling optimization of energy systems. She obtained her BSc in Electrical Engineering from Central South University, where she developed a strong foundation in energy technologies and system analysis. Her research aims to enhance the operational efficiency and flexibility of energy systems by leveraging advanced optimization algorithms and decision-making strategies.